Finite Element Simulation of Impacting Behavior of Particles in Cold Spraying by Eulerian Approach

M. Yu, W.-Y. Li, F.F. Wang, and H.L. Liao

(Submitted September 9, 2011; in revised form November 25, 2011)

In this study, an investigation on the impacting behavior of cold-sprayed particles using the Eulerian formulation available in ABAQUS/Explicit was conducted with typical copper material. The results show that a jet cannot be formed at an impact velocity less than about 290 m/s, while a continuous jet composed of both particle and substrate materials begins to initially form at about 290 m/s and a maximum equivalent plastic strain plateau can be found, which could be the approximate critical velocity. In addition, the jet presents discontinuities and the splashing causes the loss of material as the impact velocity exceeds the velocity extent of 290-400 m/s. Therefore, through theoretical analysis of the jet morphology, the Eulerian model could provide a prediction of the critical velocity.

1. Introduction

In cold spraying (CS) (also termed kinetic spraying), solid powder particles (generally 5-50 μm in diameter) are injected into a gas stream at the inlet of a converging/ diverging de-Laval-type nozzle to attain high velocity before impacting upon a substrate. If the velocity exceeds a so-called critical velocity, a transition from erosion or rebound to deposition occurs. In other words, sufficient kinetic energy must be available to plastically deform the solid material and/or disrupt the surface oxide films to achieve deposition (Ref 1-3). This critical velocity depends

M. Yu, State Key Laboratory of Solidification Processing, Shaanxi Key Laboratory of Friction Welding Technologies, Northwestern Polytechnical University, Xi'an 710072, People's Republic of China and LERMPS, Université de Technologie de Belfort-Montbéliard, Site de Sévenans, 90010 Belfort Cedex, France; and **W.-Y. Li** and **F.F. Wang**, State Key Laboratory of Solidification Processing, Shaanxi Key Laboratory of Friction Welding Technologies, Northwestern Polytechnical University, Xi'an 710072, People's Republic of China; and **H.L. Liao**, LERMPS, Université de Technologie de Belfort-Montbéliard, Site de Sévenans, 90010 Belfort Cedex, France. Contact e-mails: min.yu@ utbm.fr and liwy@nwpu.edu.cn.

not only on the type of spray material, but also on the powder quality, particle size and impact temperature. In addition, from the view of simulations, a controversial viewpoint appears that a successful bonding between the particle and substrate requires adiabatic shear instability (ASI) occurring at the local interface. Assadi et al. (Ref 4) initially put forward that the occurrence of ASI corresponded to the critical velocity obtained by using the ABAQUS software with the Lagrangian formulation. Following Assadi et al. (Ref 4) and Grujicic et al. (Ref 5), Schmidt et al. (Ref 6) further improved the Lagrangian model with the consideration of the effects of particle size and heat conduction and proposed the erosion velocity and the minimal particle impact velocity necessary to produce ASI. Undoubtedly, this Lagrangian model can obtain abundant deformation information, i.e., shape, temperature, stress and strain. Although the Lagrangian model could manifest the ASI phenomenon and quantitatively describe the critical velocity, still the dependence of simulation outputs on the element distortion could not be ignored considering the extensive plastic deformation and large shear strain gradient in CS. Based on this, the LS-DYNA (Ref 7-9), the smoothed-particle hydrodynamics (SPH) method (Ref 10) used by Li et al. (Ref 11) and the Eulerian method (Ref 12) were employed to ameliorate the issues associated with the severe mesh distortion. The simulation outputs of these methods presented comparable deformation features with the experiments. But the lack of steep change of plastic strain associated with ASI proposed by Assadi et al. (Ref 4) would not facilitate understanding the bonding mechanism in CS and quantitatively describing the critical velocity.

As for the Eulerian method, the overall mesh can be considered as two overlapping meshes, consisting of a background spatial mesh, which is fixed in space, and material, which can flow through the fixed mesh (Ref 13). Therefore, it can avoid the extreme distortion of elements,

and the Eulerian formulation on the impacting behavior is necessary due to the clearly extensive plastic deformation involved in CS.

Some examples of its applications can be found in hypervelocity impact (Ref 14) and powder forming processes (Ref 15). In addition, Yin et al. (Ref 12) pointed out that the particle deformation behavior calculated by the Eulerian method was more comparable to the experiments than that determined by the Lagrangian method.

Therefore, in the present study, an Eulerian model was developed to investigate the impacting behavior of CS particles, attempting to reveal the critical velocity and explore the bonding mechanism in CS.

2. Model Description

2.1 Finite Element Method

The impacting behavior of a copper particle on a copper substrate was simulated using an explicit FEA program ABAQUS/Explicit with the Eulerian formulation available in Version 6.8 (Dassault Systèmes Simulia Corp., Providence, Rhode Island, United States). A three-dimensional model was established, for the only available Eulerian element is the three-dimensional, 8-node element EC3D8R in ABAQUS/Explicit (Ref 16). A slice with a thickness of 1 μm was cut from the middle of the entity model and simplified as a symmetric geometry to reduce computational cost (Ref 5). Therefore, as shown in Fig. 1, a 1/2 symmetric model including a semicircular particle with 20 μm in diameter and a rectangular substrate (having a width four times the particle diameter and a height three times) was adopted. The meshing was conducted with a mesh size of 0.2 μm (a meshing resolution of $1/100d_p$).
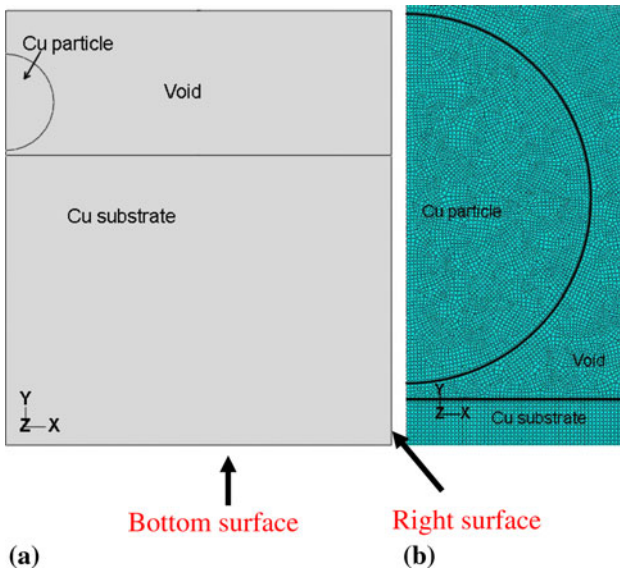
Fig. 1 (a) Symmetric model and computational domain of Cu particle (20 μm) impinging on Cu substrate under the Eulerian frame and (b) the enlarged view of elements around the particle with a meshing resolution of $1/100d_p$. Note that void material was used for other region

2.2 Material Property and Other Parameter Settings

The material flow behavior of the Cu particle and substrate was described by the Johnson-Cook plasticity model (Ref 17). The flow stress σ is a function of strain hardening, strain rate hardening and temperature softening and expressed as follows:

$$\sigma = (A + B\varepsilon^n)\left[1 + C\ln\left(1 + \frac{\dot{\varepsilon}}{\dot{\varepsilon}_0}\right)\right]\left(1 - \left[\frac{T - T_{room}}{T_{melt} - T_{room}}\right]^m\right)$$

(Eq 1)

where ε and $\dot{\varepsilon}$ are the strain and strain rate, respectively, $\dot{\varepsilon}_0$ the reference strain rate, T_{room} the reference temperature, T_{melt} the melting point. A, B, n, C and m the constants dependent on material. These constants for Cu are 90 MPa, 292 MPa, 0.31, 0.025 and 1.09 (Ref 4, 18), respectively.

A linear Mie-Gruneisen equation of state (EOS) was employed for the elastic behavior of Cu. The linear Us-Up Hugoniot form is defined as (Ref 16):

$$p = \frac{\rho_0 C_0^2 \eta}{(1 - S\eta)^2}\left(1 - \frac{\Gamma_0}{2}\eta\right) + \Gamma_0\rho_0 E_m$$

(Eq 2)

where, $\eta = 1 - \rho/\rho_0$ is the nominal volumetric compressive strain, ρ_0 the initial density, ρ the current density, C_0 the bulk speed of sound, Γ_0 the material constant named Gruneisen's gamma, S the linear Hugoniot slope coefficient, E_m the internal energy per unit reference specific volume. The variables C_0, S and Γ_0 used for Cu are 3940 m/s, 1.49 and 2.02 (Ref 12), respectively.

2.3 Governing Equations

The conservative equations in the Eulerian description are written using the spatial time derivative. The mass, momentum and energy equations are (Ref 19):

$$\frac{d\rho}{dt} = -\rho\frac{\partial u}{\partial x}$$

(Eq 3)

$$\frac{dE}{dt} = \frac{1}{\rho}\sigma_{ij}\frac{\partial u}{\partial x}$$

(Eq 4)

$$\frac{du}{dt} = \frac{1}{\partial\rho}\frac{\partial\sigma_y}{\partial x}$$

(Eq 5)

where ρ is the density, σ the Cauchy stress, u the material velocity and E the total energy per unit volume. The total energy E is the sum of the kinetic energy and the internal energy e

$$E = \frac{1}{2}\rho u \cdot u + e$$

(Eq 6)

2.4 Boundary Conditions

The Eulerian model was divided into three parts: Cu particle, Cu substrate and void. In the present model, the bottom and right surfaces of the substrate were completely fixed. The particle/substrate impact process was also

assumed to be an adiabatic process according to Assadi et al. (Ref 4). All calculations were carried out assuming that both the particle and substrate are initially at room temperature (25 °C). Finally, the elements experiencing the maximum equivalent plastic strain (PEEQ) during impact were monitored by a Python script code for outputs.

3. Results and Discussion

3.1 Evolution of Particle and Substrate Shapes at 310 m/s

A typical evolution of the particle and the substrate shapes at an initial velocity of 310 m/s is shown in Fig. 2(a)-(e). These figures show that as the particle/substrate contact time increases, the particle aspect ratio (height-to-width) decreases, while the substrate crater depth and width increase. Additionally, it can be found from Fig. 2(a) at the impact time of 5 ns that a narrow interfacial region has experienced intensive deformation

and accordingly the interfacial temperature rises. It is interesting to note that the maximum PEEQ and TEMP zones are concentrated on the surrounding of the contact zone rather than at the center of initial impact point. As the particle impact progresses, a jet composed of both the particle and substrate materials is formed at the particle/substrate interface and the particle has flattened to form a lens-like shape, as shown in Fig. 2(b). Subsequently, more particle and substrate materials are squeezed out to form the jet. The typical evolution of the jet with the impact time is shown in Fig. 2(c)-(e). Figure 2(f) shows evolutions of the maximum PEEQ and TEMP with the impact time. From this figure, it can be found that similar to literature (Ref 11), the ASI is not clearly detected solely by the occurrence of a steep change of the temperature and plastic strain evolution.

3.2 Effect of Impact Velocity

Many experimental observations show that the particle deformation is a strong function of the impact velocity
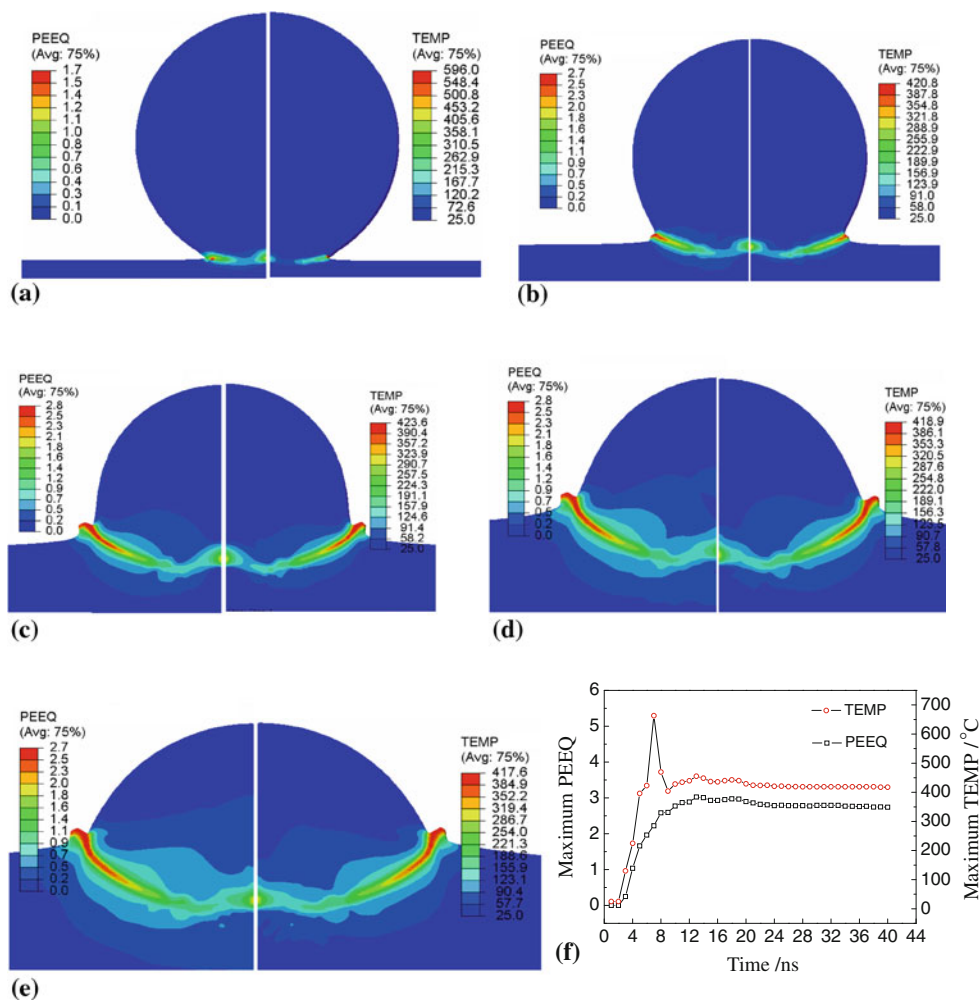

Fig. 2 Evolutions of equivalent plastic strain (PEEQ, left side) and temperature (TEMP, right side) of a 20 μm Cu particle impacting upon a Cu substrate at the impacting velocity of 310 m/s at the impacting times: (a) 5 ns, (b) 10 ns, (c) 20 ns, (d) 30 ns, (e) 40 ns and (f) evolutions of the calculated maximum PEEQ and TEMP with the impact time

(Ref 20-22). The crater volume and the flattening ratio of particles increase significantly with increasing the impact velocity (Ref 22). The calculated results are consistent with these experimental observations. Figure 3 shows the simulated contours of PEEQ after impacting at different velocities. Some conclusions could be clearly observed that the particle has deformed more extensively with increasing the velocity from 200 to 700 m/s; consequently, the depth of the crater and the flattening ratio of particles are increased. Detailed examination of the calculated outputs reveal that, at relatively low impact velocities such as 200-280 m/s as shown in Fig. 3(a)-(c), the maximum PEEQ zones are trapped by the particle and substrate materials. When the impact velocity increases to about 290 m/s, the

high strain zone is extruded in a plasticized state to form a jet as shown in Fig. 3(d). Subsequently, the jet gets elongated with the increase of velocity as shown in Fig. 3(e)-(i). However, with the impact velocity further increasing, the jet is no longer continuous and a material fracture at the jet front is observed as shown in Fig. 3(j)-(l).

3.3 Discussion on the Bonding Mechanism in Cold Spraying

The particle/substrate bonding in CS is presumed to be the result of extensive plastic deformation and related phenomena at the interface. Thus the bonding mechanism can be comparable to explosive welding, where the
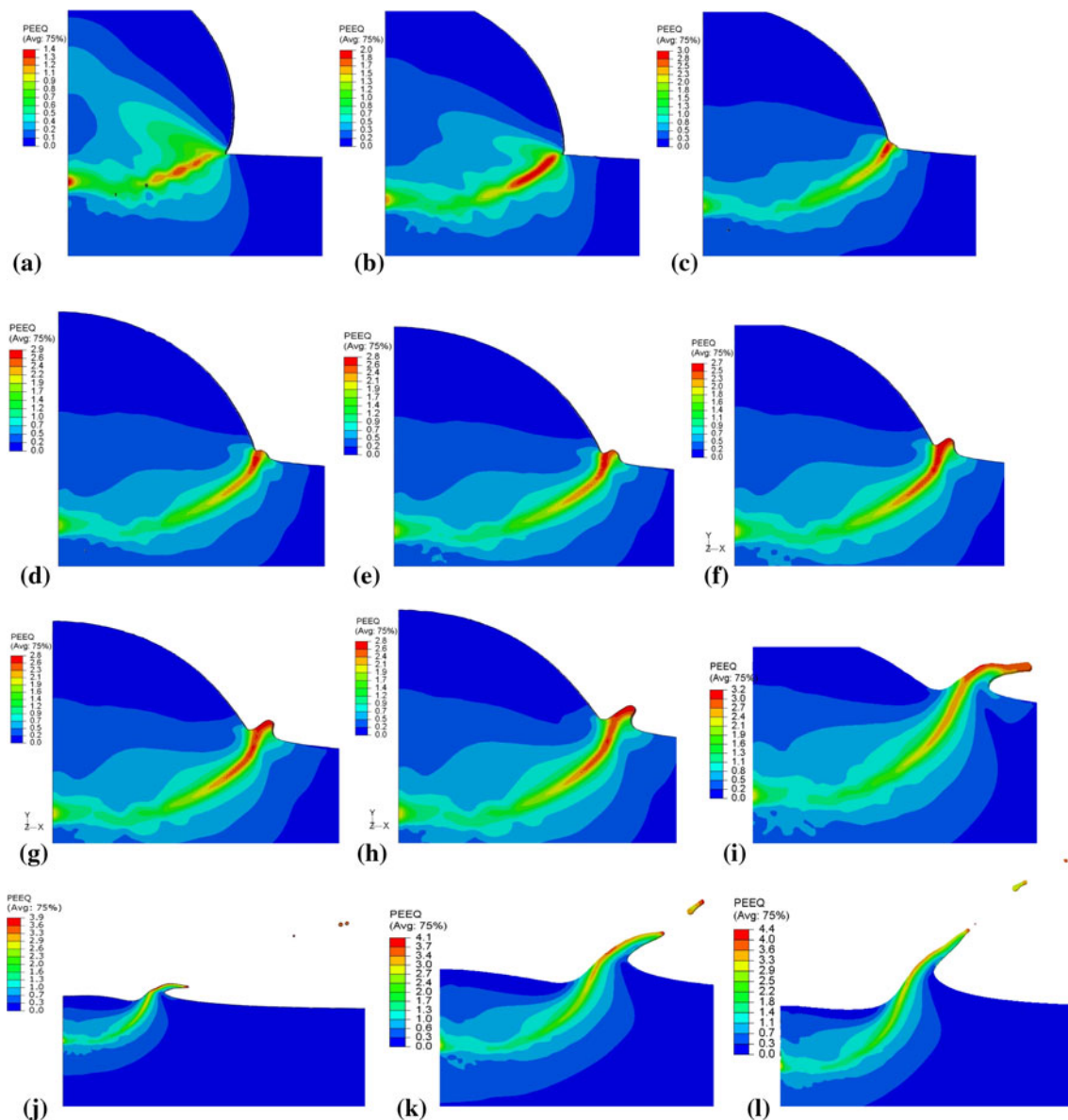
Fig. 3 Simulated contours of PEEQ after impacting of a 20 μm Cu particle upon a Cu substrate at different impacting velocities: (a) 200 m/s, (b) 250 m/s, (c) 280 m/s, (d) 290 m/s, (e) 300 m/s, (f) 310 m/s, (g) 320 m/s, (h) 330 m/s, (i) 400 m/s, (j) 500 m/s, (k) 600 m/s and (l) 700 m/s

formation of a jet at the interface is often considered as a criterion for a successful bonding (Ref 4). Assadi et al. (Ref 4) also pointed out that the calculated results using the Lagrangian method clearly illustrate the formation of a jet at the interface for the particle impacting on a rigid substrate and less prominently for the same material substrate; however, the jet prominently depends on the mesh and its onset could occur over a wide range of impact velocities, thus making the criterion ineffective (Ref 4). The jet formation obtained using the Eulerian method may be a manifestation for the critical velocity due to the independence of the Eulerian method on the mesh. The next step would be to obtain a more precise evaluation of the particle impact velocity corresponding to the jet formation. The results calculated above in Sect. 3.2 (as shown in Fig. 3) outline a window of conditions for this to take place.

As the impact velocity is in the range of 200-280 m/s (see Fig. 3a-c), a jet cannot be observed and the maximum PEEQ zone is surrounded by the particle/substrate interface, in other words, a relatively large deformation force is impeded, which could be a ''spring back'' force that may break up the initial partial bonding. The corresponding experimental phenomena could be that this particle rebounds from the substrate or creates a crater as shown in Fig. 4(a) (Ref 23), and the observation of non-adhering particles leaving craters in the substrate without any indication of a jet was also found by Assadi et al. (Ref 4). Therefore, bonding conditions are not achieved, and a jet could not be formed.

As the impact velocity increases to about 290 m/s, a jet composed of the particle and substrate material commences being formed as shown in Fig 3(d). Both the experiments (Ref 23) and Assadi et al. (Ref 4) found that as a particle adhered to the substrate, an obvious jet presented in the periphery of the adhered particle as shown in Fig. 4(b). In addition, different critical velocities for Cu particles measured by the simulations and corresponding experimental methods have been reported as 580 m/s (Ref 4), 500 m/s (Ref 6) and 550 m/s (Ref 18) for a 25 μm diameter particle through using the Lagrangian method. Other experiments have reported critical velocities of 570 m/s (Ref 24), 550 m/s (Ref 25) and 640 m/s

(Ref 26) with the oxygen content of 0.1, 0.2 and 0.336 wt.%, respectively. It has been argued that the oxide film can explain the discrepancies in the critical velocity (Ref 7). Moreover, both Kang et al. (Ref 27) and Li et al. (Ref 28) concluded that a higher feedstock oxygen content would lead to a higher critical velocity. Besides, the previous results reported the critical velocity of 310 m/s with the oxygen content of 0.02 wt.% (Ref 7) and the critical velocity of 300 m/s for a 20 μm Cu particle impacting on the copper substrate by extrapolating the shear instability velocity to a zero meshing size (Ref 7, 8). Therefore, it is rationally predicted that the velocity of 290 m/s could be the critical velocity, since the oxide films were not considered in the present study. Correspondingly, the jet formation may be a manifestation of a successful bonding. Subsequently, when the impact velocity is in the range of about 290-400 m/s, the elongating jet shown in Fig. 3(e)-(i) may tamp the bonding of the particle and substrate.

As the impact velocity surpasses the range of 290-400 m/s as shown in Fig. 3(j)-(l), the jet is no longer continuous and the jet splashing causes the loss of material. This phenomenon is consistent with the experimental results obtained by Schmidt et al. (Ref 6). Figure 5 shows the comparison of the simulated deformation patterns with the experiment observations in the literature (Ref 6). It indicates that the simulated deformation patterns are consistent with those of the experimental observations, which validates the reliability of the present Eulerian model. Additionally, the experimental phenomena of obvious cracks and erosion caused by the high velocity could be characterized by the non-continuous jet as shown in Fig. 5(c) and (d). The strong erosion would be generated as the impact velocity exceeds the upper-limit velocity for particle deposition. Therefore, the jet splashing may be a forecasting of the erosion limit and hydrodynamic penetration.

On the other hand, according to Assadi et al. (Ref 4), the critical velocity is the onset of ASI which is manifested by a jump in strain and temperature. Figure 6(a) shows the evolution of maximum PEEQ with the impact time at several typical impact velocities. It can be seen from Fig. 6(a) that, at the early impact process, the maximum PEEQ increases with the impact time and subsequently

**(a)**   **(b)**
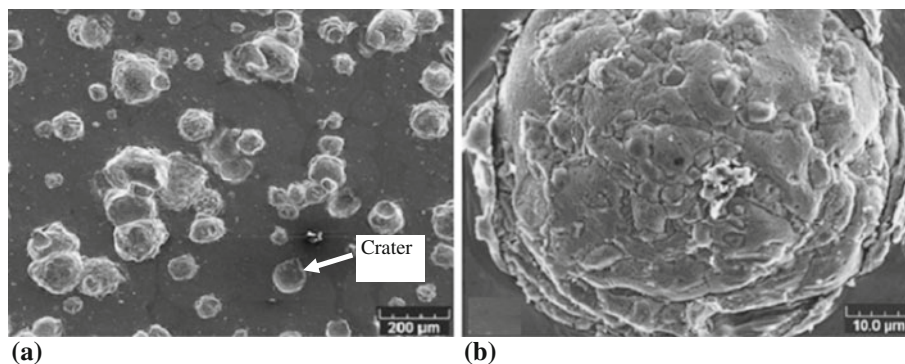
Fig. 4 (a) Surface morphology of Cu particles impinging on Cu substrate showing deposited particles and craters and (b) a single impact at high magnification (Ref 18)
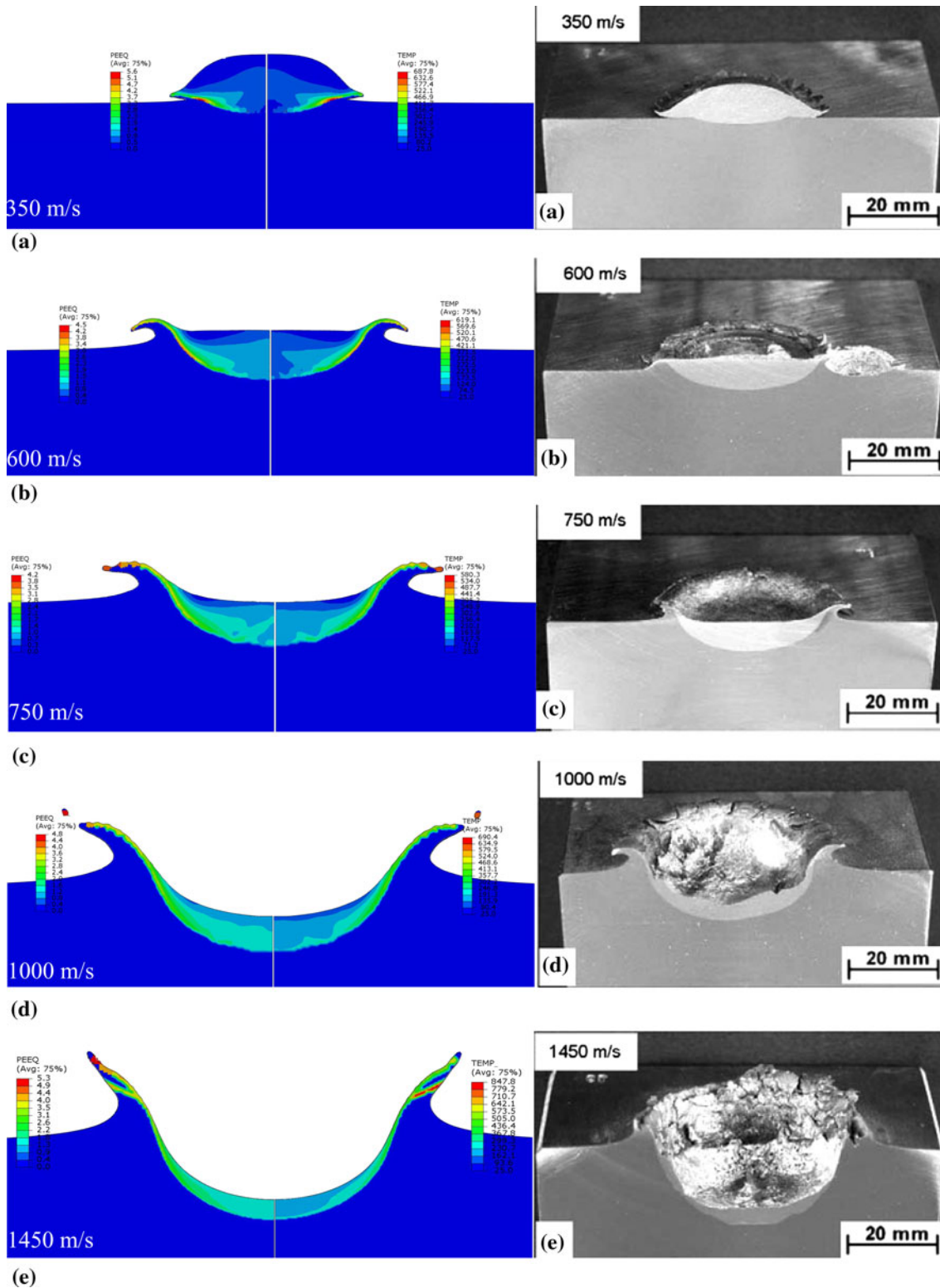
Fig. 5 Comparison of simulated shapes of a 20 mm Cu particle impacting on 20 steel substrate with macro pictures of cross-sections of 20 mm Cu ball impacting on low carbon steel plate (Ref 6) with velocities: (a) 350 m/s, (b) 600 m/s, (c) 750 m/s, (d) 1000 m/s and (e) 1450 m/s

reaches a steady state for all the impact velocities. No phenomenon associated with ASI can be clearly detected solely by the occurrence of a steep change of plastic strain

evolution as similar to the literature (Ref 11). However, Zener and Holoman (Ref 29) explained ASI to be thermoplastic instability, which means the growth and decline
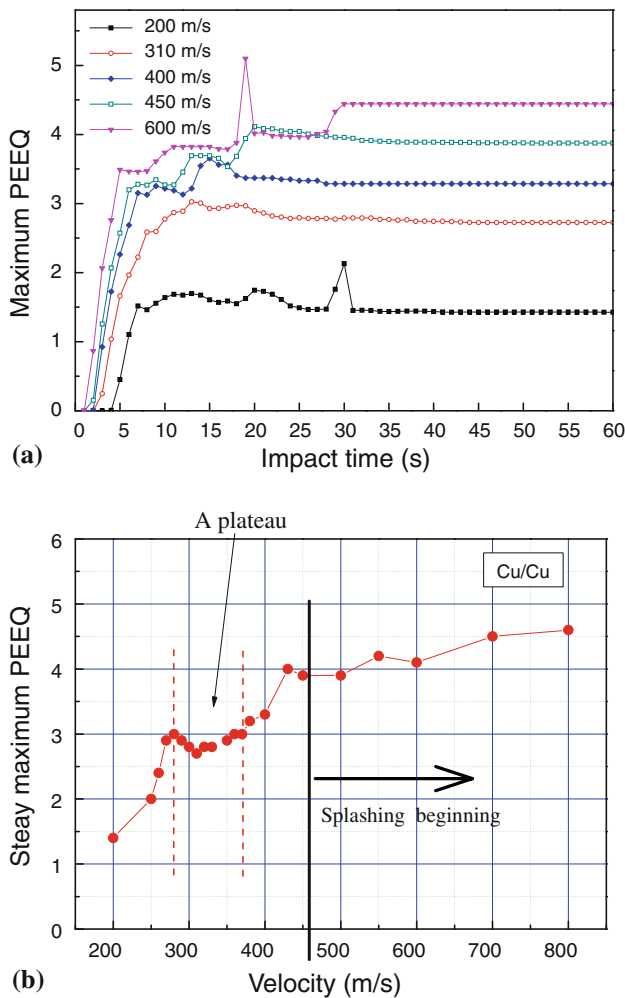
Fig. 6 (a) Evolution of maximum equivalent plastic strain (PEEQ) of a 20 μm Cu particle impacting upon a Cu substrate at different velocities and (b) effect of impact velocity on the steady maximum PEEQ

of plastic strain hardening and adiabatic thermal softening. The latter theory can be reflected in the present Eulerian model as shown in Fig. 6. Figure 6(b) shows the effect of impact velocity on the steady maximum PEEQ, which offers a window of conditions for studying the deformation characteristics. Firstly, as the impact velocity is less than 290 m/s, the steady maximum PEEQ increases linearly with the velocity, which suggests that the plastic strain hardening dominates the local deformation process. Secondly, the steady maximum PEEQ almost plateaus at the velocity range of 290-400 m/s, which could suggest a "dynamic balance" between the plastic strain hardening and adiabatic thermal softening, resulting in a stable plastic impact process. Thus the transition velocity could be the critical velocity, e.g., 290 m/s in the present model. Finally, the steady maximum PEEQ continues to increase with further increasing the velocity. The jet splashing begins at about 450 m/s and becomes severe at a velocity higher than 700 m/s compared with the erosion velocity of about 930 m/s in the literature (Ref 6). As the jet splashing

has arisen, the balance is broken by the increased impact velocity and the plastic impact may have transferred to hydrodynamic penetration until material damage in the form of the jet caused intense erosion, thus the transition point velocity, e.g., 400 m/s in the present model, could be the upper limit velocity.

4. Conclusions

The present work demonstrates the deformation process of a 20 μm diameter copper particle impacting on the same material substrate in CS using the Eulerian formulation available in the ABAQUS software. The effect of the impact velocity on the outputs for Cu were explored. Based on these results, the critical velocity could be defined as that which supports the initial formation of a jet during the impact process. In addition, as the impact velocity continuously increased, the jet was no longer continuous and the jet splashing caused the loss of material. Overall, the Eulerian model could provide a prediction of the impact velocity through theoretical analysis of the jet morphology.

Acknowledgments

References

1. H. Fukanuma, N. Ohno, B. Sun, and R.Z. Huang, In-Flight Particle Velocity Measurements with DPV-2000 in Cold Spray, *Surf. Coat. Technol.*, 2006, **5**(201), p 1935-1941
2. C.K.S. Moy, J. Cairney, G. Ranzi, M. Jahedi, and S.P. Ringer, Investigating the Microstructure and Composition of Cold Gas-Dynamic Spray (CGDS) Ti Powder Deposited on Al 6063 Substrate, *Surf. Coat. Technol.*, 2010, **23**(204), p 3739-3749
3. A. Papyrin, Cold Spray Technology, *Adv. Mater. Process*, 2001, **9**(159), p 49-51
4. H. Assadi, F. Gartner, T. Stoltenhoff, and H. Kreye, Bonding Mechanism in Cold Gas Spraying, *Acta Mater.*, 2003, **15**(51), p 4379-4394
5. M. Grujicic, C.L. Zhao, W.S. DeRosset, and D. Helfritch, Adiabatic Shear Instability Based Mechanism for Particles/Substrate Bonding in the Cold-Gas Dynamic-Spray Process, *Mater. Des.*, 2004, **8**(25), p 681-688
6. T. Schmidt, F. Gartner, H. Assadi, and H. Kreye, Development of a Generalized Parameter Window for Cold Spray Deposition, *Acta Mater.*, 2006, **3**(54), p 729-742
7. C.J. Li, W.Y. Li, and H.L. Liao, Examination of the Critical Velocity for Deposition of Particles in Cold Spraying, *J. Therm. Spray Technol.*, 2006, **2**(15), p 212-222
8. W.Y. Li, H.L. Liao, C.J. Li, H.S. Bang, and C. Coddet, Numerical Simulation of Deformation Behavior of Al Particles Impacting on

Al Substrate and Effect of Surface Oxide Films on Interfacial Bonding in Cold Spraying, *Appl. Surf. Sci.*, 2007, **11**(253), p 5084-5509

9. W.Y. Li, H.L. Liao, C.J. Li, G. Li, C. Coddet, and X.F. Wang, On High Velocity Impact of Micro-Sized Metallic Particles in Cold Spraying, *Appl. Surf. Sci.*, 2006, **5**(253), p 2852-2862

10. Y. Michel, J.M. Chevalier, C. Durin, C. Espinosa, F. Malaise, and J.J. Barrau, Meshless Modelling of Dynamic Behaviour of Glasses Under Intense Shock Loadings: Application to Matter Ejection During High Velocity Impacts on Thin Brittle Targets, *J. Phys. IV*, 2006, **134**, p 1077-1083

11. W.Y. Li, S. Yin, and X.F. Wang, Numerical Investigations of the Effect of Oblique Impact on Particle Deformation in Cold Spraying by the SPH Method, *Appl. Surf. Sci.*, 2010, **12**(256), p 3725-3734

12. S. Yin, X.F. Wang, B.P. Xu, and W.Y. Li, Examination on the Calculation Method for Modeling the Multi-Particle Impact Process in Cold Spraying, *J. Therm. Spray Technol.*, 2010, **5**(19), p 1032-1041

13. J.T. Carroll and J.S. Strenkowski, Finite-Element Models of Orthogonal Cutting with Application to Single Point Diamond Turning, *Int. J. Mech. Sci.*, 1988, **12**(30), p 899-920

14. S.R. Beissel and G.R. Johnson, Hypervelocity Impact Computation with Finite Elements and Meshfree Particles, *Int. J. Impact Eng.*, 2006, **33**, p 89-90

15. A.R. Khoei, A.R. Azami, M. Anahid, and R.W. Lewis, A Three-Invariant Hardening Plasticity for Numerical Simulation of Powder Forming Processes via the Arbitrary Lagrangian-Eulerian FE Model, *Int. J. Numer. Methods Eng.*, 2006, **5**(66), p 843-877

16. *Abaqus Analysis User's Manual*, ABAQUS 6.8 HTML Documentation, Dassault Systèmes, 2008

17. W.Y. Li and W. Gao, Some Aspects on 3D Numerical Modeling of High Velocity Impact of Particles in Cold Spraying by Explicit Finite Element Analysis, *Appl. Surf. Sci.*, 2009, **18**(255), p 7878-7892

18. G. Bae, Y. Xiong, S. Kumar, K. Kang, and C. Lee, General Aspects of Interface Bonding in Kinetic Sprayed Coatings, *Acta Mater.*, 2008, **17**(56), p 4858-4868

19. D.J. Benson and S. Okazawa, Contact in a Multi-Material Eulerian Finite Element Formulation, *Comput. Methods Appl. Mech. Eng.*, 2004, **193**(39-41), p 4277-4298

20. R.C. Dykhuizen, M.F. Smith, D.L. Gilmore, R.A. Neiser, X. Jiang, and S. Sampath, Impact of High Velocity Cold Spray Particles, *J. Therm. Spray Technol.*, 1999, **4**(8), p 559-564

21. J. Vlcek, L. Gimeno, H. Huber, and E. Lugscheider, A Systematic Approach to Material Eligibility for the Cold Spray Processes, *Mater. Lett.*, 2004, **58**, p 37-44

22. S.H. Zahiri, D. Fraser, S. Gulizia, and M. Jahedi, Effect of Processing Conditions on Porosity Formation in Cold Gas Dynamic Spraying of Copper, *J. Therm. Spray Technol.*, 2005, **3**(15), p 422-430

23. W.Y. Li, X.P. Guo, M. Yu, H.L. Liao, and C. Coddet, Investigation of Impact Behavior of Cold-Sprayed Large Annealed Copper Particles and Characterization of Coatings, *J. Therm. Spray Technol.*, 2011, **20**(1-2), p 252-259

24. T. Stoltenhoff, J. Voyer, and H. Kreye, Cold Spraying: State of the Art and Applicability, *International Thermal Spray Conference*, E.L.C.C. Berndt, Ed., 2002 (Essen, Germany), 2002, p 366-374

25. F. Gärtner, T. Stoltenhoff, T. Schmidt, and H. Kreye, The Cold Spray Process and Its Potential for Industrial Applications, *Thermal Spray Connects: Explore Its Surfacing Potential*, E. Lugscheider, Ed., DVS Deutscher Verband fur Schweißen, 2005 (Basel, Switzerland), 2005, p 158-163

26. D.L. Gilmore, R.C. Dykhuizen, R.A. Neiser, T.J. Roemer, and M.F. Smith, Particle Velocity and Deposition Efficiency in the Cold Spray Process, *J. Therm. Spray Technol.*, 1999, **4**(8), p 576-582

27. K. Kang, S. Yoon, Y. Ji, and C. Lee, Oxidation Dependency of Critical Velocity for Aluminum Feedstock Deposition in Kinetic Spraying Process, *Mater. Sci. Eng. A*, 2008, **1-2**(486), p 300-307

28. C.J. Li, H.T. Wang, Q. Zhang, G.J. Yang, W.Y. Li, and H.L. Liao, Influence of Spray Materials and Their Surface Oxidation on the Critical Velocity in Cold Spray, *J. Therm. Spray Technol.*, 2010, **19**(1-2), p 95-101

29. C. Zener and J.H. Holoman, Effect of Strain Rate upon Plastic Flow of Steels, *J. Appl. Phys.*, 1944, **15**, p 22-32